Journal of Nano- and Electronic Physics
Vol. **10** No 2, 02021(6pp) (2018)

Журнал нано- та електронної фізики
Том **10** № 2, 02021(6cc) (2018)

Modelling Graphene-based Transparent Electrodes for Si Solar Cells by Artificial Neural Networks

Z. Meziani*, Z. Dibi

University of Batna2, Advanced Electronic Laboratory (LEA), Avenue Mohamed El-Hadi Boukhlouf, 05000 Batna, Algeria

(Received 14 November 2017; published online 29 April 2018)

Transparent electrodes based on conductive transparent oxides (TCO) are increasingly invading the photovoltaic (PV) field because of their unique ability to reconcile high transparency with good electrical conductivity. The TCO market is dominated by the Indium oxide doped with Tin (ITO) with a resistivity of 30-80 Ω/sq and a transmittance of 90 % in the visible range. Yet, its cost is rising due to the high indium content, is one of the reason that encouraging research on alternative materials essential for the development of PV technologies. It is in this theme that graphene, a material with exceptional properties, is tested as a design material for transparent electrodes for Si solar cells. In this paper, we optimized optically and electronically the graphene-based transparent electrodes (G-TE) by proposing a model of simulation based on artificial intelligence and specifically artificial neural networks (ANN) which is the ANN-model. Therefore, to achieve an appropriate characterisation of a behaviour of G-TE for the Si solar cells, the ANN model has been performed to simulate and optimise different parameters of the G-TE, by controlling graphene layer number, tuning graphene work function, and deduce the suitable transmittance and resistivity in order to have a complete adjustment for these parameters. Our study mentioned that a G-TE with three layers of graphene and a work function of 4.75 eV leads for a sheet resistance of 50 Ω/sq and transmittance of 91.4 %; these results suggest that G-TE is a promising candidate in the TCO field.

Keywords: Graphene, Transparent electrodes, Indium Tin oxide, Si solar cells, ANN model.

DOI: 10.21272/jnep.10(2).02021 PACS numbers: 84.60.Jt, 81.05.Zx, 84.35. + i

1. INTRODUCTION

The cost of photovoltaic technology is mainly related to the cost of the materials used and the cost of the manufacturing process. One of the most expensive materials is that used for the fabrication of the transparent electrode. A material commonly used as a transparent electrode in PV devices is ITO, which has excellent electrical and optical properties and can be produced on a large scale [1]. However, the large scarcity of indium reserves and a significant increase in demand has led to an increase in the price of indium. Therefore, exploration of new materials for transparent electrode applications is necessary to achieve low cost and high efficiency. Potential replacement materials include metal grids [2], metal oxides [3], and thin film metals [4]. Low sheet resistivity and high optical transmittance are the fundamental requirements for these electrodes. Currently, neither ITO nor the alternative electrodes satisfy the industry's future requirements.

Graphene, a two-dimensional material made up of a monolayer of carbon atoms oriented in a hexagonal network, has attracted a great deal of scientific attention since its discovery in 2004 by K.S. Novoselov and A.K. Geim [5]. This is due to its exceptional properties, such as electronic mobility greater than 200 000 $cm^2 \cdot V^{-1} \cdot s^{-1}$ [5] and mechanical properties by making a flexible and extremely resistant material [6]. Moreover, the high transparency of a graphene monolayer, 97.7 % [7], makes it possible to envisage it as transparent electrodes for solar cells.

Experimental studies have been performed to optimize the characteristic of the sheet of graphene used as solar cells transparent electrodes, for that several parameters are studied: layer number of graphene, resistivity, transmittance, doping status; the stake is to find the adequate recombination of this parameters which gives us better results.

In this paper, a theoretical model is presented to simulate the performance of G-TE for solar cells using artificial intelligence interpreted by the ANN-model. Using parameters extracted from experiments, our simulation gives consistent results with tested performance. Based on our theoretical analysis, two practical optimization treatments have been proposed: the work function (*WF*) and layer number (*N*) of graphene should be carefully adjusted and thereafter deduce the transmittance (*T*) and sheet resistance (R_{sh}) of our G-TE.

2. GRAPHENE AND ITS APPLICATION AS TRANSPARENT ELECTRODES IN PV

2.1 Graphene Physics

Graphene is defined as a single layer of carbon atoms arranged in a hexagonal lattice. Its atomic structure can also be used as a basic building block to construct other carbon-based materials (Fig. 1a): it can be folded into fullerenes (zero-dimensional: 0D), rolled up into carbon nanotubes CNT (one-dimensional: 1D), or stacked into graphite (three dimensional: 3D). This carbon allotropes are all bonded by various combinations of the four $2s^2 2p^2$ orbital valence electrons of each carbon atom.

In graphene (two dimensional: 2D), a carbon atom shares electrons with three nearest neighbours, in the

* meziani_zahra@hotmail.fr

form of three sp^2 bonds, leaving out-of-plane p_z orbitals with one electron per atom. The three electrons forming the sp^2 bonds are responsible for the outstanding mechanical and thermal properties of graphene (Fig. 1b)

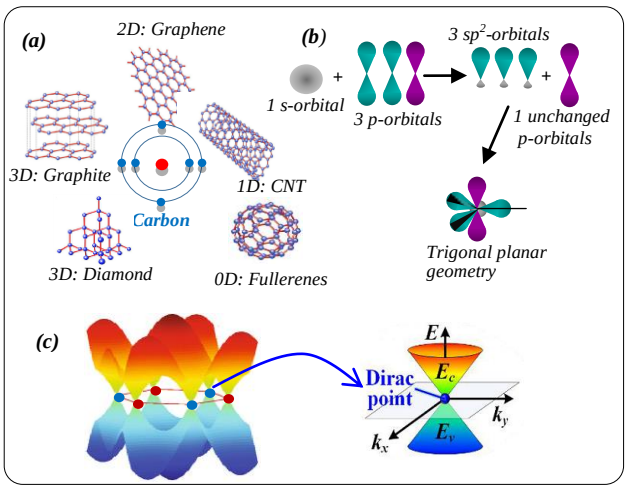

Fig. 1 – (a) Schematic of carbon atom and carbon allotropes, from 0D to 3D; (b) atomic orbitals of graphene; (c) energy dispersion of graphene, where the energy dispersion is linear for low energies near the six corners (Dirac points) of the two-dimensional hexagonal Brillouin zone

On the other hand, the electrons in the p_z orbitals can easily hop between the neighbouring atoms, since the hopping energy is high (~ 3.0 eV), and thus form the π bands in the conduction bands (Ec) and π^* bands in the valence bands (Ev). These electrons contribute to the outstanding electrical properties of graphene. As shown in Figure 1c, Ec and Ev meet at the six corners of the first Brillouin zone (named as Dirac points) resulting in a zero bandgap. Hence, graphene behaves like a semi-metal [5].

2.2 Graphene Preparation and Transfer

Graphene can be fabricated mainly by two techniques. Physical technique-which involves:

- Micromechanical exfoliation of highly ordered pyrolytic graphite (HOPG) [5], with this technique we obtain samples of high crystalline quality but their dimensions are inadequate to use as a transparent electrodes (samples in order of micrometre).
- Sublimation of silicon from SiC at high temperatures [8], but the high cost of SiC substrates is the major inconvenient to use this method for producing G-TE.

Chemical technique-which involves:

- Reduction of graphene oxide [5-9], the electrical properties of these films are lower.
- Chemical vapor deposition (CVD) on metal catalyst substrates [10].

The CVD method produce large- scale and high quality of graphene. In this method, usually, Cu foil or Ni layers are used as the catalyst, and CH_4 is used as the carbon source with H_2 as the carrier gas. The synthesized graphene is usually transferred to the device substrate with the help of a polymer PMMA [poly (methyl methacrylate)]. It is reported that graphene synthesized by CVD electrically and optically outperforms ITO [11] and thus is promising in serving as a transparent conductive film.

With the growth of graphene on copper, we obtain samples of more than 95 % monolayer graphene [12]. The use of monolayer graphene makes it possible to have a better control over the transparency of the electrodes produced by stacking several layers of graphene.

Despite the exceptional mechanical properties of graphene [6], its thickness of a few atomic layers makes it very difficult to transfer its samples (on the order of centimetre) without causing rupture to the graphene. For this reason, most graphene transfers are carried out by adding the PMMA.

For the step of metal sheet dissolution, different chemical solutions are used: solution of $FeCl_3$ or HCl used for nickel sheet, and a solution of Fe $(NO_3)_3$ used for copper sheet. When the metal sheet is completely dissolved, the graphene film floating on the surface of the solution is then rinsed in deionized water and recovered directly on the desired substrate. The samples are then dried. It is then possible to remove the PMMA by immersing the samples in acetone.

2.3 Graphene/Semiconductor Schottky Junction

Because of the near-zero band-gap and high conductivity characteristics of graphene, the graphene/n-type semiconductor heterojunction can be taken as a metal/semiconductor Schottky junction (assuming the work function difference between the graphene and the semiconductor is large enough). Recently, several studies proposed a photovoltaic model in which highly conductive, transparent graphene films is coated on n-type silicon (n-Si) wafer to form Schottky junction [13]. The results of these studies showed that in this Schottky solar cell, graphene as energy conversion materials not only contributes to charge separation and transport, but also functions as transparent electrode.

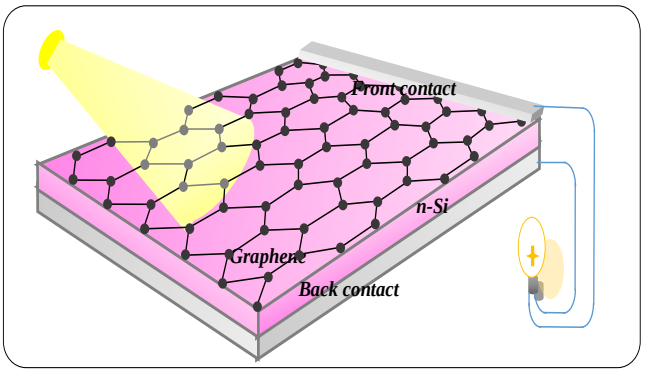

Fig. 2 – A graphene/semiconductor photovoltaic device

The mechanism of such Schottky junction solar cell can be understood qualitatively by plotting the energy band diagram. Figure 3a shows the energy diagram of a graphene/n-Si Schottky junction solar cell under illumination. Due to the work function difference between the graphene (ϕ_G), and semiconductor (ϕ_S), a built-in potential forms in the semiconductor near the interface. Under light illumination above the bandgap, the photogenerated holes and electrons are separated and driven towards the Schottky electrode (graphene

film) and semiconductor layer, respectively, by the built-in electric field. We assume that the junction between graphene and semiconductor is an ideal Schottky contact, so the built-in potential ϕ_{bi} equals to the work function difference of these two materials:

$$\phi_{bi} = \phi_G - \phi_S = \phi_G - \chi - k\,T\ln(N_D/N_C) \qquad (1)$$

Where χ is the semiconductor electron affinity, N_D and N_C are the doping and the effective electron state concentration of semiconductor, respectively. As graphene is metallic, *n*-type silicon is chosen as the substrate to obtain a comparatively large built-in potential. If the graphene *WF* becomes larger, a stronger electric field will be formed on the semiconductor side of the junction, hence improving the junction's capacity to collect photo-generated carriers. The mechanism of tuning the *WF* of graphene is rather straight forward. As shown in Figure 3.b, the dispersion of mobile π electrons in monolayer graphene near the Dirac point in the first Brillouin zone is in a linear correlation. For intrinsic graphene, the Fermi energy is located at the crossing point of the π and π^* bands, which renders the carrier density at a low level. However, if the Fermi energy is shifted away from the original position (Fig. 3c), more electrons or holes can be activated to participate in the conduction process. Therefore, graphene with shifted Fermi energy (i.e., modulated *WF*) performs better in conducting.

The *WF* of graphene can be tuned either by an applied electric field or by proper chemical doping. For example, $AuCl_3$ doping can improve the *WF* to as high as 5.1 eV. After chemical doping, the transmittance *T* is almost unchangeable, furthermore, the sheet resistance R_{sh} has rapidly decreased after chemical doping [13], and a several analysis of the dependence of R_{sh} on *WF* [13], from which it is known that R_{sh} decreases significantly upon a tiny shift of *WF* from its intrinsic state.

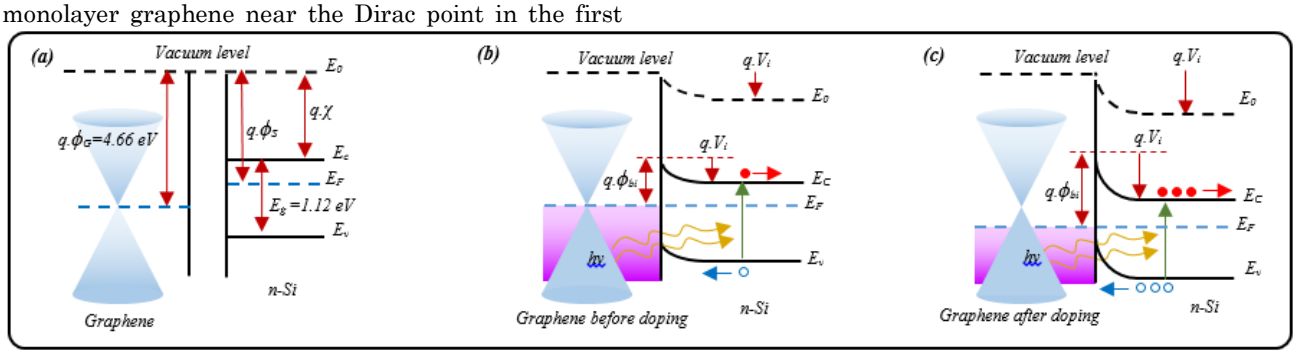

Fig. 3 – (a) The energy band diagram of the graphene and n-Si semiconductor, (b) The energy band diagram of the graphene/*n*-Si Schottky junction before doping graphene, (c) after doping graphene

3. CHARACTERISATION OF G-TE WITH ANN

The objective of this work is to create an ANN model that can faithfully reproduce the response of the solar cells G-TE. For this, we must determine parameters that have influences on the performance of the G-TE, and thereafter we dispatch up theme into input parameters and output parameters. We have to optimise the transmittance and the sheet resistance of our G-TE by controlling the layer number and the work function of graphene.

3.1 ANN Model Designing

The ANN model of our design process can be summarised in these stages [14-15-16]:

- Collecting a database characterised by the input and output parameters.
- Separation of the database into three subsets (training base, validation base and test base).
- The choice of the architecture of the ANN (Selection of inputs, outputs, number of hidden layers, number of neurons per layer, the activation functions ...).
- Training the neural network on the bases of Training and validation.
- Measurement of neural network performance on the test base.

Our study focuses on the recent research on G-TE and all the graphene involved in this highlights are synthesized by the CVD method on copper foils.

3.2 Collecting the Database

The database includes the ANN inputs and associated outputs, and therefore it determines both network size (and hence the simulation time) and performance. For our training, we have used different curves, associating each value of *N* and *WF* of graphene an R_{sh} or *T* value of G-TE.

To realize our ANN model the database is composed of 1390 elements divided into 03 sub-base: training base, validation base and test base.

It should be noted here that there are no specific rules concerning this separation, however, in general the training set must include a significant percentage of the given base that can exceed 60 %, for validation base it represents between 20 % and 30 % of the database, and finally the test base is between 10 % and 25 % of the database, depending on the problem at hand [15-16]. In our work the training base is composed of 834 elements (60 %), the validation base is composed of 417 elements (30 %) and the test base is composed of 139 elements (10 %). It is important to not use any element of the test base during the training. This database is available only to the final performance measurement.

3.3 Choice of the Architecture of the ANN

We can make a classification for an ANN according to its architecture, training selected and the activation

function used. The simplest and most known of ANN and most used for approximation and prediction problems is the multilayer perceptron (MLP) [15]. It consists of several neural layers generally connected in a feed forward structure. The calculation of the output is done by propagating the calculations from left to right, with a supervised training. The activation function used is primarily the Sigmoïd function [15-16]. To drive the MLP, the training algorithm used is usually the algorithm of back propagation. According to [15-16] an MLP with two hidden layer having a Sigmoïdal activation function in the first layer and a linear function in the output layer, allows one to approximate the function studied with acceptable accuracy, provided you have enough neurons on hidden layers (Fig. 4).

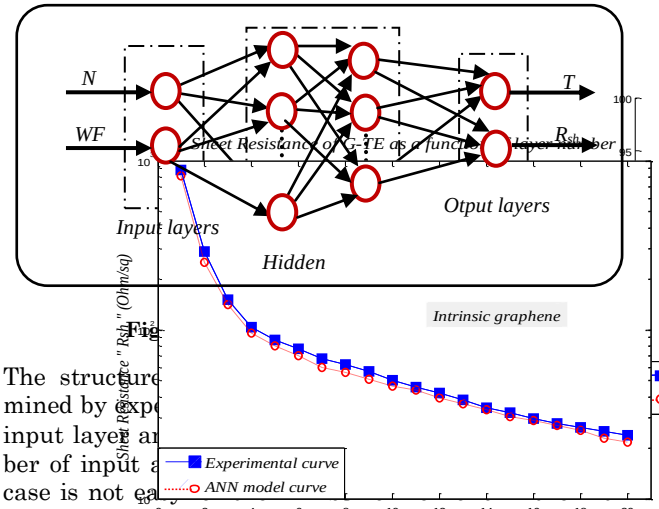

Fig. – The structure
mined by exp
input layer a
ber of input
case is not ea
den. In fact, with a limited number of neurons, the network will not be performing on training, and with a number of excessive weight, the network may have poor generalisation properties (phenomenon of overtraining).The solution to remedy to this problem is to build multiple architectures and select the most suitable model for our application. We retain the architecture that gives the minimum mean square error (MSE).

4. RESULTS AND DISCUSSION

Once all training steps are performed, our MLP is formed and performance measures compared to experimental data is needed to test the reliability of our ANN model, for this we cross to the test phase.

4.1 Test Phase and Measuring the Performance of the ANN Model

In this phase, it is necessary to carry out tests to estimate the quality of the generalisation. Figure 5 shows the performance of the ANN model obtained for the curves used, the solid lines plot the experimental data and the dashed lines present our simulation interpreted by our ANN model. The layer number N is an important parameter that influences both the transmittance T and the sheet resistance R_{sh} of graphene, and thus determines the G-TE performance. Figure 5a and 5b plot T and R_{sh} of intrinsic graphene as a function of N, respectively, using the experimental values and our simulation. As the layer number increases, the sheet

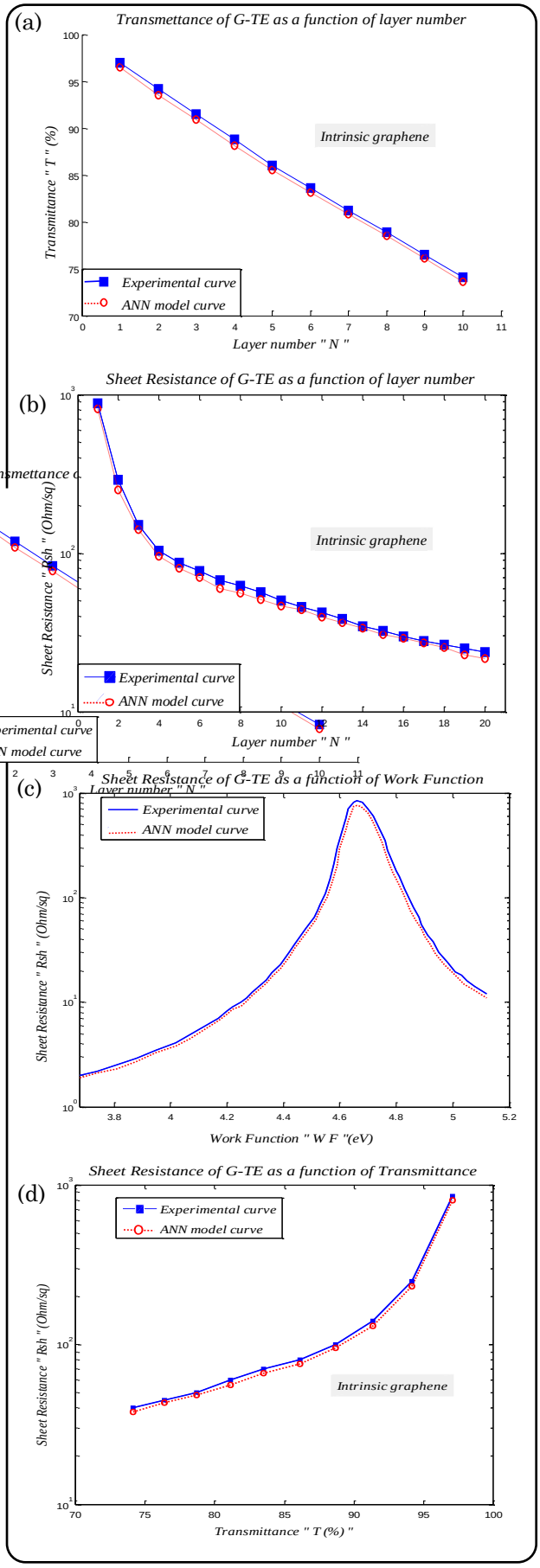

Fig. 5 – ANN Model Performance for the different training curves

resistance decreases dramatically, which improves the G-TE performance, but the graphene film becomes less transparent, which in turn offsets the gains in G-TE performance. Figure 5c shows the analysis of the dependence of R_{sh} on the *WF*, R_{sh} decreases upon a tiny shift of *WF* from its intrinsic value (4.66e V). Figure 5d summarizes the R_{sh}-*T* curves of both the reported experimental data and our simulation results. The comparison between the original database and that obtained after training the ANN model indicates that the data obtained by the MLP are very close to the experimental values and our ANN model expresses faithfully the behaviour of the G-TE.

4.2 Prediction of G-TE Behaviour with the ANN Model

The performance of our ANN model is tested for inputs that have not been confronted by our system when training. In this phase the ANN model predict the behaviour of the G-TE with different input values.

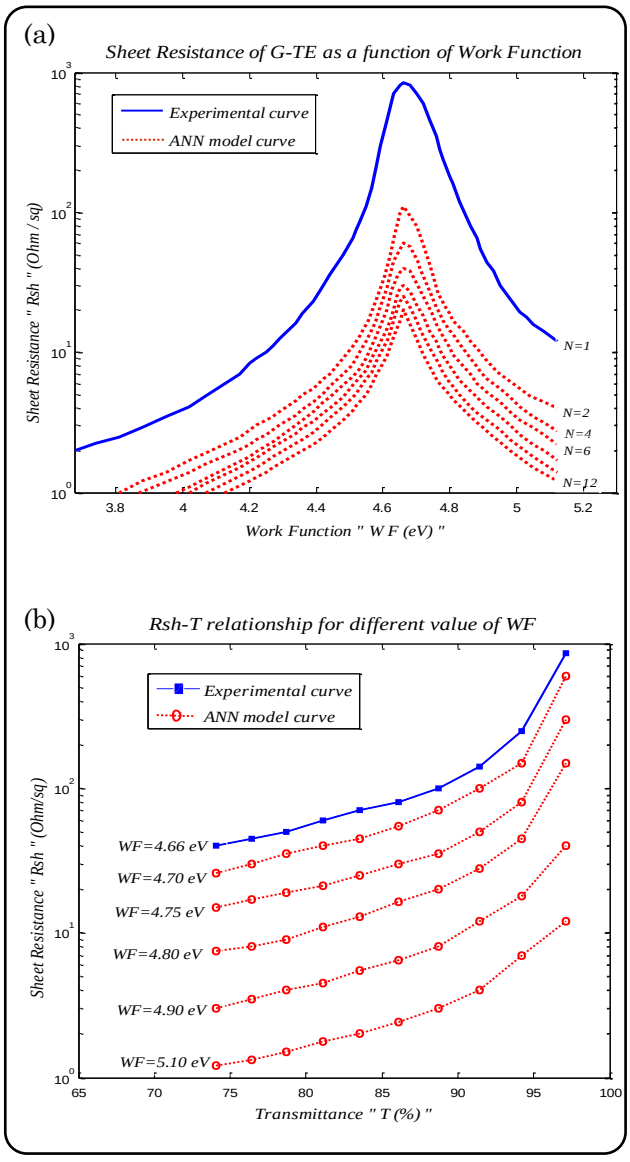

Fig. 6 – ANN model prediction of G-TE behaviour

Once the validity of the proposed method for G-TE behaviour has been verified, this methodology has been used to obtain different curves $R_{sh}(WF)$ for different *N* values as shown in Figure 6a and $R_{sh}(T)$ for different *WF* values as shown in Figure 6b. Our simulation are presented in dashed lines. The solid lines plot the experimental data.

The engineering of work function *WF* and layer number *N* of graphene plays an important role to affect the final device performance. As shown in figure 6 the proposed model with the artificial neural networks provide an accurate prediction for the curves $R_{sh}(WF)$ for different *N* values and $R_{sh}(T)$ for different *WF* values of the G-TE. Our MLP was correctly trained; it tends to give reasonable responses. In table1, we selected input values who lead to output parameters close to ITO performance (resistivity of 30-80 Ω/sq and a transmittance of 90 %).

Table 1 – Description of the selected parameters

Input Parameters		Output Parameters	
N	*WF* (eV)	*T* (%)	R_{sh} (Ω/sq)
1	4.90	97.1	50
1	5.10	97.1	16
2	4.75	94.2	80
2	4.80	94.2	45
2	4.90	94.2	18
2	5.10	94.2	7
3	4.70	91.4	100
3	4.75	91.4	50
3	4.80	91.4	28
3	4.90	91.4	12
3	5.10	91.4	4
4	4.70	88.7	70
4	4.75	88.7	38
4	4.80	88.7	20
4	4.90	88.7	8
4	5.10	88.7	3

5. CONCLUSION

The work presented in this article relates to the G-TE modelling with artificial neural networks is a very useful tool for PV system designers, because it gives a useful combination of the properties of graphene as transparent conducting electrodes in Si Schottky solar cells, which provides high electrical conductivity and good optical transparency.

In comparison to similar solar cell devices using ITO as electrodes, G-TE solar cells can deliver comparable photovoltaic performance. It is found that with three layers of graphene and a work function of 4.75 eV leads to a sheet resistance of 50 Ω/sq and transmittance of 91.4 %.

The theoretical predictions with the ANN model suggest that several recombination of input parameters are validated, however a compromise between this in-

puts and the G-TE production cost is an important point to study. With the projected predictions, the G-TE can be expected to pass the industry requirement for the next generation of TCO, including application in solar cells.

REFERENCES

1. S. Bae, H. Kim, Y. Lee, X. Xu, J.S. Park, Y. Zheng, J. alakrishnan, T. Lei, H.R. Kim, Y.I. Song, Y.J. Kim, K.S. Kim, B. Ozyilmaz, J.H. Ahn, B.H. Hong, S. Iijima, *Nat. Nanotechnol.* **5** No 8, 574 (2010).
2. K. Tvingstedt, O. Inganäs, *Adv. Mater.* **19** No 19, 2893 (2007).
3. V. Bhosle, J. T. Prater, F. Yang, D. Burk, S.R. Forrest, J. Narayan, *J. Appl. Phys.* **102** No 2, 023501 (2007).
4. B.O'Connor, C. Haughn, K.H. An, K.P. Pipe, M. Shtein, *Appl. Phys. Lett.* **93** No 22, 223304 (2008).
5. K.S. Novoselov, A.K. Geim, S.V. Morozov, D. Jiang, Y. Zhang, S.V. Dubonos, I.V. Grigorieva, A.A. Firsov, *Science* **306** No 5696, 666 (2004).
6. C. Lee, X. Wei, J.W. Kysar, J. Hone, *Science* **321** No 5887, 385 (2008).
7. R. R. Nair, P. Blake, A.N. Grigorenko, K.S. Novoselov, T.J. Booth, T. Stauber, N.M.R. Peres, A.K. Geim, *Science* **320** No 5881, 1308 (2008).
8. K.V. Emtsev, A. Bostwick, K. Horn, J. Jobst, G.L. Kellogg, L. Ley, J.L. McChesney, T. Ohta, S.A. Reshanov, J. Röhrl, E. Rotenberg, A.K. Schmid, D. Waldmann, H.B. Weber, T. Seyller, *Nat. Mater.* **8** No 3, 203 (2009).
9. S. Stankovich, D.A. Dikin, R.D. Piner, K.A. Kohlhaas, A. Kleinhammes, Y. Jia, Y. Wue, S.B.T. Nguyen, R.S. Ruoff, *Carbon* **45**, 1558 (2007).
10. A. Reina, X. Jia, J. Ho, D. Nezich, H. Son, V. Bulovic, M.S. Dresselhaus, J. Kong, *Nano. Lett.* **9** No 1, 30 (2009).
11. F. Bonaccorso, Z. Sun, T. Hasan, A.C. Ferrari, *Nat. Photon.* **4**, 611 (2010).
12. M. Biron, *Croissance et transfert de graphène pour la fabrication d'électrodes transparentes* (Canada: Univ. of Montreal: 2013).
13. Y.C. Lai, B.S. Wu, S.C. Yu, P.Yu, G.C. Chi, *IEEE* **978**, 2436 (2013).
14. F. Junod, M. Bornoz, *A la découverte des réseaux de neurones.* (Switzerland: Univ of Yverdon : 2002).
15. M. Parizeau, *Réseaux de neurones*. (France: Univ of Laval: 2006).
16. Z. Meziani, Z. Dibi, *Afr. J. Sci. Tech. Innov. Develop.* **8** No 4, 331 (2016).